Assessment of LES and RANS turbulence models with measurements in liquid metal GaInSn model of continuous casting process

R. Chaudhary, C. Ji, and B.G. Thomas

Department of Mechanical Science & Engineering

University of Illinois at Urbana-Champaign,

Urbana, IL, USA

Abstract

Continuous casting of steel requires optimization of mean and fluctuation velocities to minimize defects. The turbulent flow in the nozzle and mold of a continuous casting process depends upon various process (casting speed, magnetic field etc.) and geometric (nozzle geometry, SEN depth etc.) parameters. To control these parameters efficiently, one needs to gain insight into the turbulent flow in these systems. The turbulence research in these systems mostly relies on computational techniques.

Realizing the importance of turbulence in these systems and the need of an accurate simulation technique, in this work, Large Eddy Simulation (LES), and Reynolds-Averaged Navier Stokes (RANS) type computational simulations have been combined with the measurements in a small scale GaInSn model in order to evaluate their performances. The results of these two simulation techniques are evaluated along with the measurements at various levels. Transient features of the turbulent flow in the nozzle and mold of the GaInSn model are studied.

LES outperformed RANS models in matching measurements. Within RANS, SKE model is found to be performing better than RKE. Both RANS models (SKE and RKE) performed reasonably well in the nozzle, especially for mean velocities. The accuracy of predictions dropped for turbulent kinetic energy when compared with LES. The mismatch between the predictions of SKE and LES increased in the mold perhaps due to dominance of low Reynolds number effects and more sophisticated slanted jet flow in the mold. The velocity fluctuations with higher frequencies and standard deviations are found to be dominating in the well and at the center of the ports of the nozzle.

Overall, based upon above work, a rationale view on the performance of RANS and LES simulation techniques in modeling of turbulent flow in continuous casting process is given.

Key words: LES, RANS, simulation, turbulent flow, mold, nozzle, continuous casting

1. INTRODUCTION

Continuous casting of steel is an energy intensive process and needs careful process optimization to minimize expensive defects in cast product. Turbulent fluid flow in the nozzle and mold of the continuous casting process is the main cause of defects related to the slag entrainment, alumina inclusion entrapment, hook formations etc [1]. Computational models combined with physical models are needed to study the complex turbulent flow features in these systems [2]. Reynolds-Averaged Navier Stokes (RANS) models and water modeling are among the most popular techniques to analyze these systems [3-6].

Relatively small number of studies exists on transient Large Eddy Simulation (LES) calculations in the nozzle and mold of continuous casting process [7-12]. Yuan et al [7] combined LES and Particle Image Velocimetry (PIV) measurements in a 0.4 scale water model. The LES predictions were found matching well with the measurements. The two types of flow patterns in the jet exiting the nozzle were observed, i.e. stair-step downward wobbling of jet and jet bending midway between narrow face and Submerged Entry Nozzle (SEN). Long term flow asymmetries were observed in the lower region of the mold. The interaction of the flow from two halves was reported causing large velocity fluctuations near the top surface. Ramos-Banderas et al [8] combined LES and digital PIV in a water model of slab caster. Simulations were reported agreeing well with the instantaneous velocity field measurements. Flow was reported changing significantly due to vertical oscillations of the jet. Turbulence was found to be inducing natural biasing without the influence of any other factors such as slide-gate, gas injection or SEN clogging. Instantaneous velocity showed periodic behavior and frequencies of this behavior was reported increasing with flow rate.

In another work, Yuan et al [9] performed LES and inclusion transport studies in a water model and thin slab caster. The time averaged flow patterns agreed well with the measurements performed using hot-wire anemometry and dye injections in a full scale water model. Complex

time varying structures were found even in nominally steady conditions. The flow in the mold was found to be switching in between double-roll flow and complex flow with many rolls. Zhao et al [10] performed LES with superheat transport and combined with plant measurements and measurements in a full scale water model. The velocity and temperature predictions matched with the dye injection measurements in the water model and with thermocouple measurements in the plant respectively. The jet exiting the nozzle showed chaotic variations with temperature fluctuations in the upper liquid pool varying $\pm 4\,^{o}C$ and heat flux $\pm 350\,kw/m^2$. Addition of static-k SGS model was found giving minor effects.

Qian et al [11] employed LES with a DC magnetic field effects in a slab continuous casting process. The effect of SEN depth and port angle on vortex formation was analyzed and the mechanism of vortex formation was outlined. A new vortex brake was proposed and its effect on vortex suppression was studied. The effect of the location of the magnetic field brake on vortex formation was also studied. The magnetic brake, when applied at free surface, suppressed turbulent and biased vortices significantly. Liu et al [12] applied LES in a continuous casting mold to study the transient flow patterns in the upper region. The turbulent asymmetry in the upper region was reported all the times. The upper transient roll was found to break into number of small scale vortices.

Although, as outlined above enough work exist on RANS, LES and water modeling but only Thomas et al [13] evaluated LES and RANS turbulent flow simulations with the measurements using PIV in a 0.4 scale water model and using electromagnetic probe in a operating slab casting machine. All simulations and measurements showed remarkable quantitative agreement for average flow patterns and velocities. In this work, during simulations, the constant Smagorinsky Sub-Grid Scale (SGS) model in LES without any wall treatment method and standard k-ε model for RANS with standard wall function approach were used.

In the absence of more work on evaluation of LES and RANS models with the measurements and the need of better LES and RANS predictions compared with the measurements during evaluation, the current work considered Wall-Adapting Local Eddy-viscosity (WALE) type SGS model [14], which gives right behavior of SGS viscosity close to wall, with a more accurate Werner-Wengle (WW) [15], as evaluated by [16], wall treatment in coarse meshes in LES

calculations. Also, in RANS, the improved k-ε model [17-18] which has a realizable formulation for Reynolds normal and shear stresses (realizable k-ε model (RKE)) and standard k-ε model (SKE) [19] with better two-layer wall treatment combined with single-blended wall function called enhanced wall treatment (EWT) [18, 20-21] is used.

Overall, in this work, LES and RANS simulations are combined with the velocity measurements performed by others [22-23] using Ultrasonic Doppler Velocimetry (UDV) in the GaInSn model of the continuous casting process. The organization of this work is as follows: initially, performance of RANS (SKE and RKE) and LES simulations is assessed by comparing simulations with the measurements for the horizontal time averaged velocity at the mold mid-plane between wide faces. Later, a more detailed comparison of LES and SKE predictions is performed in the nozzle and mold of the GaInSn model of continuous casting process. Afterwards, the transient histories of velocity predicted by LES simulations are analyzed in more details. Overall, based upon above work, the performance of LES and RANS is evaluated at different levels to be used in the simulation of the nozzle and mold of the continuous casting process.

2. FORMULATIONS

A. LES

The 3-D time dependent Navier-Stokes (N-S) equations can be filtered and the velocities can be decomposed into resolved and subgrid velocities. Based upon the filtering procedure, the filtered N-S equation can be written as [24],

$$\frac{\partial \bar{u}_i}{\partial t} + \frac{\partial \bar{u}_i \bar{u}_j}{\partial x_j} = -\frac{1}{\rho}\frac{\partial \bar{p}}{\partial x_i} + \frac{\partial}{\partial x_j}\left(\nu \frac{\partial \bar{u}_i}{\partial x_j}\right) - \frac{\partial \tau_{ij}}{\partial x_j} \tag{1}$$

Where, $\tau_{ij} \equiv \overline{u_i u_j} - \bar{u}_i \bar{u}_j$ are the subgrid stresses. The subgrid stresses can be modeled in terms of mean velocities and Sub-Grid Scale (SGS) viscosity (ν_s) as [25],

$$\tau_{ij} - \frac{1}{3}\tau_{kk}\delta_{ij} = -2\nu_s \bar{S}_{ij}, \text{ where, } \bar{S}_{ij} = \frac{1}{2}\left(\frac{\partial \bar{u}_i}{\partial x_j} + \frac{\partial \bar{u}_j}{\partial x_i}\right) \tag{2}$$

There are various models available to close SGS viscosity in the above equation. Constant Smagorinsky model [26], dynamic Smagorinsky-Lilly model [27-29], dynamic kinetic energy sub-grid scale model [30] and Wall-Adapting Local Eddy-viscosity model (WALE) [14] are some of the SGS viscosity models popular in widespread applications. Among these models, WALE is mathematically more reasonable and accurate in flows involving complicated geometries [14]. The best part in this model is that it recovers the y^3 behavior of eddy viscosity close to the wall without any expensive and complicated dynamic procedure [14]. In constant Smagorinsky model, the van-driest damping is usually used to give proper near wall behavior in SGS viscosity. Van-Driest damping when used with constant Smagorinsky model gives y^2 behavior and not y^3 [14]. Besides, the application of Van-Driest damping in complicated geometries is difficult due to difficulty in defining y+ in the domain [14]. Due to above mentioned reasons and the requirement of proper behavior of SGS viscosity in complicated wall bounded geometry, especially with coarse meshes at the nozzle bottom. The WALE SGS model is used in the current work. The SGS viscosity in the WALE model is defined as [14],

$$\nu_s = L_s^2 \frac{\left(S_{ij}^d S_{ij}^d\right)^{3/2}}{\left(\bar{S}_{ij}\bar{S}_{ij}\right)^{5/2} + \left(S_{ij}^d S_{ij}^d\right)^{5/4}} \tag{3}$$

$$S_{ij}^d = \frac{1}{2}\left(\bar{g}_{ij}^2 + \bar{g}_{ji}^2\right) - \frac{1}{3}\delta_{ij}\bar{g}_{kk}^2,\ \bar{g}_{ij} = \frac{\partial \bar{u}_i}{\partial x_j},\ \delta_{ij} = 1,\ \text{if i=j, else } \delta_{ij} = 0$$

$L_s = \min\left(\kappa d, C_w \Delta\right)$, where $\Delta = \left(\Delta x \Delta y \Delta z\right)^{1/3}$, $\kappa = 0.418$, $C_w = 0.325$, d is distance from cell center to the closest wall. Δx, Δy, and Δz are the grid spacing in x, y and z directions.

B. RANS

In RANS approach, the ensemble averaging on instantaneous N-S equations is performed in order to obtain averaged N-S equations. The averaged N-S equations can be written as [24]:

$$\frac{\partial \bar{u}_i}{\partial t} + \frac{\partial \bar{u}_i \bar{u}_j}{\partial x_j} = -\frac{1}{\rho}\frac{\partial \bar{p}}{\partial x_i} + \frac{\partial}{\partial x_j}\left(\nu \frac{\partial \bar{u}_i}{\partial x_j}\right) + \frac{\partial R_{ij}}{\partial x_j} \tag{4}$$

Where, $R_{ij} = -\overline{u_i' u_j'}$ are the Reynolds stresses. There are total nine components of Reynolds stresses and six of them are independent. In k-ε type turbulence models, Boussinesq hypothesis is usually used to close Reynolds stresses via mean velocity and eddy viscosity [24-25].

$$R_{ij} = -\overline{u_i' u_j'} = \nu_{\mathrm{t}} \left(\frac{\partial \overline{u}_i}{\partial x_j} + \frac{\partial \overline{u}_j}{\partial x_i} \right) - \frac{2}{3} k \delta_{ij} \tag{5}$$

There are various two-equation turbulence models currently available to close eddy viscosity (ν_{t}) in above equation. Among them are the RKE and SKE which are used in the current work. More details on these two models and their formulations can be found in [31] and [18].

C. Wall treatment

In LES calculations, due to a relatively coarse mesh for turbulent flow at Re~47,000 (based upon nozzle bore diameter and bulk axial velocity) in the nozzle, a wall function approach given by Werner-Wengle [15] is used. This wall treatment method integrates a linear and a power law profile for instantaneous tangential velocity in near wall cells to relate the cell average instantaneous tangential velocity with the cell average instantaneous wall shear stress. In this formulation, the following velocity profiles are used.

$$u^+ = \frac{\overline{u}}{u_\tau} = \begin{cases} y^+ = \dfrac{\rho u_\tau y}{\mu} & y^+ < 11.8 \\ A\left(y^+\right)^B & y^+ > 11.8 \end{cases}$$

Upon integration of above profiles over the cell width perpendicular to wall in the cells next to wall and taking $\tau_w = \rho u_\tau^2$ (where τ_w is wall shear stress) the cell averaged instantaneous velocity in the cell next to wall can be related to the cell average instantaneous wall shear stress as follows [18];

$$|\tau_w| = \begin{cases} \dfrac{2\mu|u_p|}{\Delta z} & |u_p| \le \dfrac{\mu}{2\rho\Delta z} A^{\frac{2}{1-B}} \\ \rho\left[\dfrac{1-B}{2} A^{\frac{1+B}{1-B}} \left(\dfrac{\mu}{\rho\Delta z}\right)^{1+B} + \dfrac{1+B}{A}\left(\dfrac{\mu}{\rho\Delta z}\right)^{B} |u_p|\right]^{\frac{2}{1+B}} & |u_p| > \dfrac{\mu}{2\rho\Delta z} A^{\frac{2}{1-B}} \end{cases}$$

$A = 8.3,\ B = 1/7$, u_p is the cell average instantaneous tangential velocity in the cell next to the wall. Δz is near wall cell thickness in wall normal direction.

In RANS (SKE and RKE) calculations, the enhanced wall treatment (EWT) as available in FLUENT is used. More details on the formulations on these wall treatment approaches are given in [18] and [31].

3. PHYSICAL AND COMPUTATIONAL DOMAINS, BOUNDARY CONDITIONS AND NUMERICAL METHODS

The velocity measurements for this work are performed in a small scale GaInSn model of continuous casting process at FZD, Dresden, Germany [22-23]. The GaInSn model has a 300 mm long nozzle with a constant inner bore of 10 mm with zero degree bifurcated ports feeding liquid metal into the mold cavity. The mold dimensions are 140 mm (width) x 35 mm (thickness) with a vertical length of 300 mm. The liquid metal free surface level is maintained around 5 mm below mold top. The liquid metal from the mold cavity flows out of mold via two side outlets each having a diameter of 20 mm. Fig-1(a) gives the front view of the GaInSn model. The bottom left figure (Fig-1(b)) shows the top view of the bottom of the system where the bottom-sides of the mold are round. Realizing minor importance of bottom region and to avoid difficulty in creating hexahedral mesh, the circular bottom regions are approximated with equal area rectangular regions as shown in Fig-1(c). More details on various dimensions, process parameters (Casting speed, flow rate etc.) and fluid properties [32] (density and viscosity) are presented in Table 1.

To minimize computational cost, the two fold symmetry of the domain was utilized and only 1/4th of the domain was used in RANS (RKE and SKE with EWT) simulations. In 1/4th combined nozzle and mold domain, a mesh of around 0.62 million hexa cells was used. Fig-2(a)

shows the isometric view of the mesh used in the RANS calculations. Fig-2(b) and (c) presents the close-up at the same mesh in the mold-mid plane around SEN bottom and around the port respectively. In LES calculations, due to it being a time dependent technique capturing full 3-D turbulence, the full domain was considered. The combined nozzle and mold in LES has similar mesh as used in RANS but with a total of ~1.33 million hexa cells.

In RANS calculations, at the inlet of the nozzle, a constant velocity ($U_m = 1.4$ m/s, equivalent to 110ml/sec flow rate) boundary condition with k and ε values of 0.01964 m^2/s^2 and 0.55 m^2/s^3 respectively calculated using formulations ($k = 0.01U_m^2$, and $\varepsilon = k^{1.5} / 0.05D$, where D is hydraulic diameter) given by [33] were used. In LES calculations, only mean velocity boundary condition (i.e. 1.4 m/s) was used without any perturbation and flow was allowed to develop turbulence in the domain.

In both LES and RANS, the top surface of the mold was taken free-slip boundary. The outlets of the mold were applied a constant pressure boundary condition (0 Pa gauge). All walls of the domain were considered no-slip. In RANS (RKE and SKE) models, the wall boundary was handled using EWT and in LES using Werner-Wengle formulation.

During RANS calculations, the ensemble averaged equations for the three momentum components, turbulent kinetic energy (k-), dissipation rate (ε-), and Pressure Poisson Equation (PPE) are discretized using the Finite Volume Method (FVM) in FLUENT [18] with 2nd -order upwind scheme for convection terms. These discretized equations are then solved for velocity and pressure using the Semi-Implicit Pressure Linked Equations (SIMPLE) algorithm, starting with initial conditions of zero velocity in the whole domain. The segregated solver in FLUENT is used to solve all equations. For convergence, the un-scaled absolute residuals in all equations are reduced below $1x10^{-04}$.

In LES calculations, the filtered N-S equations are discretized again using FVM in FLUENT with 2nd-order central differencing scheme for convection terms. The time integration is achieved using 2nd order implicit scheme. The velocity-pressure coupling is obtained using Implicit Fractional Step Method (I-FSM). The time dependent LES calculations were started with zero velocity fields in the whole domain and flow was allowed to develop for 23.56 sec before

starting collecting time statistics. Time statistics were collected for 21.48 sec with a $\Delta t = 0.0002$ sec. Every timestep, the un-scaled residuals on continuity and momentum equations were reduced by more than 3 orders of magnitude.

All computations (RANS and LES) were performed on a PC with a 2.66 GHz Intel® Xeon processor (Intel Corp., Santa Clara, US) and 8.0 GB RAM. This machine has a total of 8 cores and in each run 6 cores were utilized. The RANS calculation in 1/4th domain (RKE and SKE with EWT) took around 8 hrs of total real time in final convergence. LES calculation in the full domain took around 26 sec per timestep update and total of 225200 timesteps to integrate for total 45.04 sec (23.56 (time in flow to develop) + 21.48 (averaging time) = 45.04) (total time taken by PC in final results ~1626 Hrs=67 days)

4. COMPARISON OF LES AND RANS PREDICTIONS WITH THE MEASUREMENTS

Fig-3 compares the average horizontal velocity in between RKE, SKE and measurements [22-23] (~0.2 sec interval data and averaged over ~25 sec total time, total ~125 frames) performed using UDV method along three horizontal lines (95, 105, and 115 mm from mold top) at the mid-plane between wide faces. Qualitatively both RKE and SKE predicted the velocity profile but SKE matched better with the measurements, especially along the lines at 105 and 115 mm from the mold top. Due to the better performance by SKE in matching measurements, it has been selected for further analysis from the two RANS models.

Fig-4 compares the 21.48 sec time-averaged horizontal velocity predicted by LES-WALE-WW model with the measurements. Measurements are inaccurate close to SEN along 95 mm line and therefore the mismatch in between LES and measurement along this line is not considered important. Otherwise, LES matched very well in the whole domain, except very close to narrow face. Very close to the narrow face all three predictions (RKE, SKE, and LES) give higher horizontal velocity than measurements. Overall, LES has outperformed the two RANS models in matching with the measurements.

The comparison of the average horizontal velocity at the mold-mid plane between measurements, LES and SKE is presented in Fig-5. As can be seen, LES captures the correct spread of the jet and matches best with the measurements. The jet from SKE is thin and directed

more towards narrow face. This behavior of SKE model is due to it being a steady state technique and therefore unable to capture the transient wobbling of the jet. Due to small number of data frames in measurements, the average values show some wiggles. As mentioned previously, the measurements close to SEN are inaccurate and therefore should not be considered for comparison.

5. RESULTS AND DISCUSSION

After realizing the accuracy of the two RANS models and LES simulations, the more accurate RANS model (i.e. SKE) and LES are considered for further comparison. The results are organized in the sequence of the various parts of the system, i.e. first results are discussed in nozzle and then in the mold. Finally, the transient behavior of the flow via instantaneous velocity magnitude collect at various points in the nozzle and mold is discussed.

A. Nozzle flow

The velocity magnitude contours and streamlines at the nozzle mid-plane at the bottom are shown in Fig-6 and 7 respectively. The flow patterns match very closely in the SKE and LES except minor differences. This close match by SKE with LES is perhaps due to high Reynolds number flow (Re~47,000, based upon nozzle bore diameter and bulk axial velocity) in nozzle for which SKE model is most suitable. The LES suggests slightly shorter region of plug flow from the nozzle bore with a steeper jet angle. Also, the back flow region in LES is slightly smaller.

The comparison of the front view of the port velocity magnitude contours and vectors is presented in Fig-8 with the jet characteristics [34] given in Table 2. As previously suggested in the nozzle-mid plane velocity contours, the LES (25%) gives smaller back flow zone than SKE (34%). The vertical jet angle predicted by LES are higher (38.5 vs 32.5) than SKE. Although, SKE suggests a bigger region of forward flow but the weighted horizontal spread angle is higher in LES (8.6 vs 5.1). This behavior is perhaps due to the up-down and right-left wobbling of the jet predicted more accurately by LES. It is interesting to note that although the average jet speed in the two is quite similar (within ~6%), but weighted vertical, horizontal and outward velocities are quite different. LES and SKE give almost same weighted vertical velocity (~8% lower), the differences in horizontal (~32% lower) and outward (~15% higher) velocity are much larger.

SKE predicts ~40% less weighted average turbulent kinetic energy than the weighted average resolved turbulent kinetic energy of LES.

The flow in the mold, which is critical to the quality of the steel, is mainly controlled by the jet therefore a more detailed comparison of velocity and turbulence coming out of ports is preformed. Fig-9 presents the comparison of velocity magnitude along the vertical lines at the port-mid and at 2 mm towards wide face from port-mid. Along the port-mid line in the strong forward flow region, all simulations (SKE, RKE and LES) agreed quite well (within ~3%). The peak velocity predicted by all models is same (~1.4 m/s). In the recirculation region at the top of the port, the RANS models predicted lower values than LES. The mismatch in the velocity is higher along 2 mm offset line. RKE and SKE predicted closely, as expected, but the LES predictions are a lot different in values from them along 2mm offset line.

The comparison of the turbulent kinetic energy, along the same lines as above at the port, predicted by SKE and LES is presented in Fig-10. As expected, the turbulent kinetic energy is much higher in the higher velocity forward flow region along both the lines; this trend is predicted by all models. The mismatch in between SKE and LES is much higher in turbulent kinetic energy (often exceeding 100%) than in velocity. The RANS models seem to be disagreeing most with LES for turbulence than mean velocities. Similar behavior of RANS models was found by Chaudhary et al [31] in square duct and channel flows when compared with Direct Numerical Simulation (DNS).

B. Mold flow

Now moving on to the mold flow, Fig-11(a) and (b) respectively present the mean velocity contours in SKE and LES at the mold mid-plane. As seen, velocity contours are quite similar in the two except few differences. The LES predicted a thicker jet showing more spread as moving into the mold cavity. The jet in SKE is thinner and more focused thus giving higher velocity at the center of the mold in the lower recirculation region. The instantaneous velocity from LES at ~45 sec is shown in Fig-11(c). The instantaneous flow patterns are consistent with the mean flow. The maximum instantaneous velocity at the mold-mid plane at ~45 sec is ~9% higher than the maximum mean.

Further, the flow patterns at the mold mid-plane are more clearly presented with the help of mean velocity streamlines in Fig-12. Fig-12(a) shows the streamlines predicted by SKE whereas Fig-12(b) and (c) respectively show the streamlines predicted by LES after 11.66 and 21.48 sec time-average. Both SKE and LES predicted classic double-roll flow with SKE suggesting stronger lower roll with its location slightly upward than LES. It is interesting to note that the flow in upper recirculation zone is quite symmetric after 11.66 sec average in LES but not in lower recirculation region. The symmetry between right and left improves with more time averaging at 21.48 sec. This behavior suggests the importance of large scale flow structures in the lower recirculation region. This finding of large scale flow dominance in lower recirculation zone is consistent with the previous work of Yuan et al [7].

The mean velocity vectors in between SKE and LES are compared at the mold-mid plane and 3 mm towards wide face from mid-plane respectively in Fig-13(a) and (b). As previously hinted but clearly seen here is that the jet is thicker in LES then SKE. SKE seems to have failed to capture the real fluctuating behavior of jet via average formulations.

Fig-14(a) compares the surface velocity predicted by SKE and LES at the mold-mid plane between wide faces. At 30 mm away from nozzle center towards narrow face, SKE and LES predicted close to each other (within ~50%). The mismatch near SEN is much higher (exceeding 200%), interestingly SKE suggested reverse flow towards narrow face in this region. Due to higher SEN depth, surface velocity is too slow, nearly 5-7 times smaller than typical caster (~0.3) [1] and therefore one of the reasons behind greater mismatch in between LES and SKE.

Fig-14(b) compares the vertical velocity along a horizontal line 35 mm below the free surface at the mold-mid plane. Due to the jet being more focused in the smaller region, SKE predicts stronger upward velocity close to narrow face (~500% stronger than LES) and stronger downward velocity close to SEN (~180% stronger than LES). The vertical velocity along a vertical line 2 mm from narrow face is compared between LES and SKE in Fig-14(c). SKE and LES both predicted same vertical jet impingement location (~110 mm from free surface) at the narrow face. Here also, SKE suggested to be predicting higher upward velocity (~70% higher than LES) close to narrow face in upper region and stronger downward velocity (~80% higher than LES) in the lower region. In the lower region, SKE shows positive velocity around 250 mm

onwards towards bottom from the free surface suggesting an early flow separation from the narrow face in SKE than in LES.

C. Transient flow in the nozzle and the mold

Finally, the time histories of the velocity magnitude collected at various points at the nozzle- and mold-mid plane are presented in Fig-15. Fig-15(a) shows the locations of various points (given with red-squares with their x, y, and z-coordinates in mm) where velocity magnitude as a function of time is presented in Fig-15(b) to (j). For points-2, 3 and points-7, 8, the time histories of velocity both right and left sides of SEN are presented. For other points, only data on the left side of SEN is given. As expected, since point 1, 4 and 6 fall in the way of strong bore and jet flow therefore point 1 has the maximum time average velocity followed by at point 4 and then 6. Other points are off from the strong momentum in the nozzle and mold domain and therefore have much lower velocity then point 1, 4 and 6. Although mean velocity is maximum at point 1, but the points 6, 2 and 3 suggested largest fluctuations around the mean values. The Point 6 has the highest (~0.29) standard deviations of the velocity fluctuations around mean followed by at point 2 (~0.25) and 3 (~0.25). The reason for points 6 having highest velocity fluctuations is due to it being in the well of the nozzle where flow changes quite violently.

The velocity at point 2, 3 and 7, 8 is quite symmetric on the right and left of the SEN. The velocity fluctuations (at points 1, 2,3 4, 6, 11 and 17) close to SEN suggest higher frequency fluctuations compared to points (at points 7, 8, 13 and 15) away from the SEN. This behavior is as per the Reynolds number in different parts of the region. The higher Reynolds number (Re~47000 in nozzle bore), inside and around nozzle, gives higher frequency fluctuations suggesting dominance of small scales. The Reynolds number in the mold is around 1/10 of in the nozzle bore (i.e. ~4215, based upon hydraulic diameter of the mold cross-section and bulk velocity) and therefore suggest low frequencies.

The mean-squared amplitude (MSA) power spectrum (formulations given in previous work [9]), which gives the distribution of energy with frequencies, for velocity fluctuations at point 6 and 15 is given in Fig-16. The general trend of having more turbulent energy at lower frequencies is consistent with previous work [5, 9]. As expected, the point 6 shows distribution of energy up to

much higher frequencies than at point 15. This behavior of velocity fluctuations is quite intuitive as per the Reynolds number.

7. CONCLUSIONS

In this work, RANS (SKE and RKE) and LES turbulence models are used with measurements in a GaInSn model of continuous casting process to understand their performances in predicting mean and turbulence parameters in different regions of the nozzle and mold. When compared with measurements in the mold for horizontal velocity, LES simulations outperformed both RANS models. Within RANS, SKE model is found to be better than RKE. Measurements close to SEN, especially along 95 mm line are not accurate therefore should not be considered for comparison.

The RANS (RKE and SKE) models matched LES reasonable well for mean velocity in the nozzle (within ~3-15% in forward flow region). The errors increased in turbulent kinetic energy predictions (often exceeding 100%). This finding is consistent with the performance of these RANS models in channel and square duct flows when compared with DNS previously [31]. The performance of RANS models for mean velocities matching closely with LES is perhaps due to high Reynolds number effects in the nozzle for which the RANS models are more suitable.

In the mold, although, both SKE and LES predicted classic double-roll flow but the velocities are a lot different in the two. The SKE predicted thinner jet penetrating into the mold giving higher upward and downward velocities after hitting the narrow face. The spread and profile of the jet was more accurately predicted by LES when compared with measurements. Interestingly, the jet impingement at narrow face predicted by both SKE and LES is same (i.e. 110 mm from free surface). The surface velocity, especially 30 mm onwards towards narrow face is reasonably matched between SKE and LES (maximum error within 50%). The mismatch close to SEN increased hugely (exceeding 200%). This higher mismatch in between SKE and LES on the free surface is perhaps due to flow being too slow in this region because of larger SEN depth.

After 11.66 sec time average, LES is found to be giving slightly asymmetric flow patterns in the lower recirculation zone. The asymmetry decreased upon more time averaging (i.e. 21.48 sec). This behavior suggests the importance of large scale flows in the lower part of the domain which

is consistent with the previous work [9]. Velocities collected at the nozzle and mold mid plane at various points is found to be giving interesting flow behavior. Higher frequencies are found to be dominating in and around the nozzle region.

Overall, this work gives an idea about the performance of the RANS and LES models in different parts of the nozzle and mold of a continuous casting process. Besides, a greater insight into the transient flow in the nozzle and mold of continuous casting process is obtained.

ACKNOWLEDGMENTS

The authors are very grateful to K. Timmel and G. Gerbeth from MHD Department, Forschungszentrum Dresden-Rossendorf (FZD), Dresden, Germany for providing the velocity measurement data in GaInSn model. This work was supported by the Continuous Casting Consortium, Department of Mechanical Science & Engineering, University of Illinois at Urbana-Champaign, IL, and ANSYS, Inc is acknowledged for providing FLUENT.

REFERENCES

(1) B. G. Thomas, Fluid flow in the mold, Chapter 14 in Making, Shaping and Treating of Steel, 11th Edition, vol. 5, Casting Volume, Editor: A. Cramb, AISE Steel Foundation, Oct. 2003, Pittsburgh, PA, pp. 14.1-14.41.

(2) B. G. Thomas, Modeling of continuous casting, Chapter 5 in Making, Shaping and Treating of Steel, 11th Edition, vol. 5, Casting Volume, Editor: A. Cramb, AISE Steel Foundation, Oct. 2003, Pittsburgh, PA, pp. 5.1-5.24.

(3) D. E. Hershey, B. G. Thomas, and F. M. Najjar, Turbulent flow through bifurcated nozzles, Int. J. Num. Meth. in Fluids, 1993, 17(1), pp. 23-47.

(4) B. G. Thomas, L. J. Mika and F. M. Najjar, Simulation of fluid flow inside a continuous slab-casting machine, Metall. Trans. B, 1990, vol. 21B, pp. 387-400.

(5) R. Chaudhary, G.-G. Lee, B. G. Thomas, and S.-H. Kim, Transient Mold Fluid Flow with Well- and Mountain-Bottom Nozzles in Continuous Casting of Steel, Metall. Mat. Trans B, 2008, vol. 39B, no. 6, pp. 870-884.

(6) X. Huang and B. G. Thomas, Modeling of transient flow phenomena in continuous casting of steel, Canadian Metallurgical Quarterly, 1998, vol. 37, no. 3-4, pp. 197-212.

(7) Q. Yuan, S. Sivaramakrishnan, S.P. Vanka and B. G. Thomas, Computational and experimental study of turbulent flow in a 0.4 scale water model of a continuous steel caster, Metall. Mat. Trans. B, 2004, vol. 35B, pp. 967-982.

(8) A. Ramos-Banderas, R. Sanchez-Perez, R. D. Morales, J. Palafox-Ramos, L. Demedices-Garcia, and M. Diaz-Cruz, Mathematical simulation and physical modeling of unsteady fluid flow in a water model of a slab mold, Metall. Mat. Trans. B, 2004, vol. 35B, pp. 449-460.

(9) Q. Yuan, B. G. Thomas and S. P. Vanka, Study of transient flow and particle transport in continuous steel caster molds: Part I. Fluid flow, Metall Mat. Trans. B, 2004, vol. 35B, pp. 685-702.

(10) B. Zhao, B. G. Thomas, S. P. Vanka and R. J. O'Malley, Transient fluid flow and superheat transport in continuous casting of steel slabs, Metall. Mat. Trans. B., 2005, vol. 36B, pp. 801-823.

(11) Z.-D. Qian and Y.-L. Wu, Large eddy simulation of turbulent flow with the effects of DC magnetic field and vortex brake application in continuous casting, ISIJ International, 2004, vol. 44, no. 1, pp. 100-107.

(12) R. Liu, W. Ji, J. Li, H. Shen, and B. Liu, Numerical simulation of transient flow patterns of upper rolls in continuous slab casting moulds, Steel Research Int., 2008, 79, no. 8, pp. 50-55.

(13) B. G. Thomas, Q. Yuan, S. Sivaramakrishnan, T. Shi, S. P. Vanka and M. B. Assar, Comparison of four methods to evaluate fluid velocities in a continuous slab casting mold, ISIJ Int., 2001, vol. 41, no. 10, pp. 1262-1271.

(14) F. Nicoud and F. Ducros, Subgrid-scale stress modeling based on the square of the velocity gradient tensor, Flow, Turbulence and Combustion, 1999, vol. 63(3), pp. 183-200.

(15) H. Werner and H. Wengle, Large-eddy simulation of turbulence flow over and around a cube in a plate channel, in 8th symposium on turbulent shear flows, 1991, Munich, Germany.

(16) L. Temmerman, M. A. Leschziner, C. P. Mellen, and J. Frohlich, Investigation of wall-function approximations and subgrid-scale models in large eddy simulation of separated flow in a channel with streamwise periodic constrictions, Int. J. Heat Fluid Flow, 2003, vol. 24, issue 2, pp. 157-180.

(17) T.-H. Shih, W. W. Liou, A. Shabbir, Z. Yang, and J. Zhu, A New k-ε Eddy-Viscosity Model for High Reynolds Number Turbulent Flows - Model Development and Validation, Computers & Fluids, 1995, vol. 24(3), pp. 227-238.

(18) FLUENT6.3-Manual (2007), ANSYS Inc., 10 Cavendish Court, Lebanon, NH, USA.

(19) B. E. Launder, and D. B. Spalding, Mathematical Models of Turbulence. 1972: London Academic Press.

(20) B. Kader, Temperature and concentration profiles in fully turbulent boundary layers, Int. J. Heat Mass Transfer, 1981, 24(9), pp. 1541-1544.

(21) M. Wolfstein, The velocity and temperature distribution of one-dimensional flow with turbulence augmentation and pressure gradient, Int. J. Heat Mass transfer, 1969, 12, pp. 301-318.

(22) K. Timmel, V. Galindo, X. Miao, S. Eckert, G. Gerbeth, Flow investigations in an isothermal liquid metal model of the continuous casting process, 6th International Conference on Electromagnetic Processing of materials (EPM), Oct. 19-23 2009, Dresden, Germany, Proceedings pp. 231-234.

(23) K. Timmel, S. Eckert, G. Gerbeth, F. Stefani, T. Wondrak, Experimental modeling of the continuous casting process of steel using low melting point alloys – the LIMMCAST program, ISIJ International, 2010, 50, No. 8, pp. 1134-1141.

(24) S. B. Pope, Turbulent Flows, 2000, Cambridge University Press, Cambridge, United Kindom.

(25) J. O. Hinze, Turbulence, McGraw-Hill Publishing Company,1975, NewYork.

(26) J. Smagorinsky, General circulation experiments with the primitive equations I. The basic experiment, Month. Wea. Rev., 1963, 92, pp. 99-164.

(27) M. Germano, U. piomelli, P. Moin, W. H. Cabot, Dynamic subgrid-scale eddy viscosity model, In summer Workshop, Center for Turbulence Research, 1996, Stanford, CA.

(28) D. K. Lilly, A proposed modification of the Germano subgrid-scale closure model, Phys. Fluids, 1992, vol. 4, pp. 633-635.

(29) S.-E. Kim, Large eddy simulation using unstructured meshes and dynamic subgrid-scale turbulence models, Technical Report AIAA-2004-2548, 34th Fluid Dynamic Conference and Exhibit, June 2004, AIAA.

(30) W.-W. Kim and S. Menon, Application of the localized dynamic subgrid-scale model to turbulent wall-bounded flows, Technical Report AIAA-97-0210, 35th Aerospace Science Meeting, Jan. 1997, AIAA.

(31) R. Chaudhary, B.G. Thomas and S.P. Vanka, Evaluation of turbulence models in MHD channel and square duct flows, Journal of Turbulence, Submitted (June 2010).

(32) N. B. Morley, J. Burris, L. C. Cadwallader, and M. D. Nornberg, GaInSn usage in the research laboratory, Review of Scientific Instruments, 79, 056107, 2008.

(33) K. Y. M. Lai, M. Salcudean, S. Tanaka and R. I. L. Guthrie, Mathematical modeling of flows in large tundish systems in steelmaking, Metall. Mat. Trans. B, 17B, 1986, pp. 449-459.

(34) Bai, H., and Thomas, B. G., Turbulent Flow of Liquid Steel and Argon Bubbles in Slide-gate Tundish Nozzles: Part I. Model Development and Validation, Metall. Mat. Trans. B, 2001, 32(2), pp. 253-267.

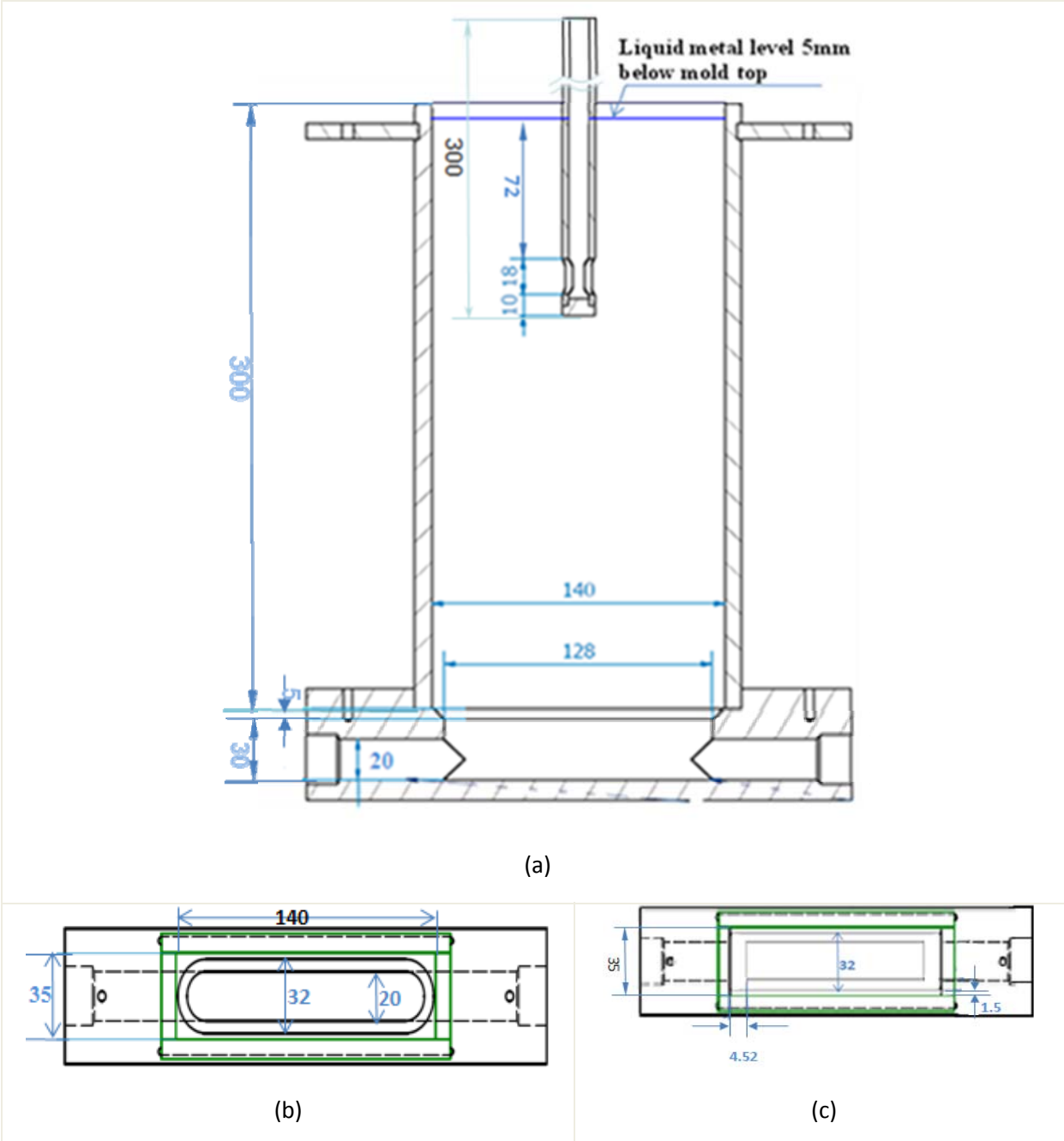

Fig-1 Geometric details on the GaInSn model of continuous casting [22-23] (a) front view of the nozzle and mold together (b) top view of the bottom region of the mold (c) top view of approximated bottom circular region with equal area rectangle (also, each outlet is 20 mm x16 mm rectangle cross-section based upon equal area concept)

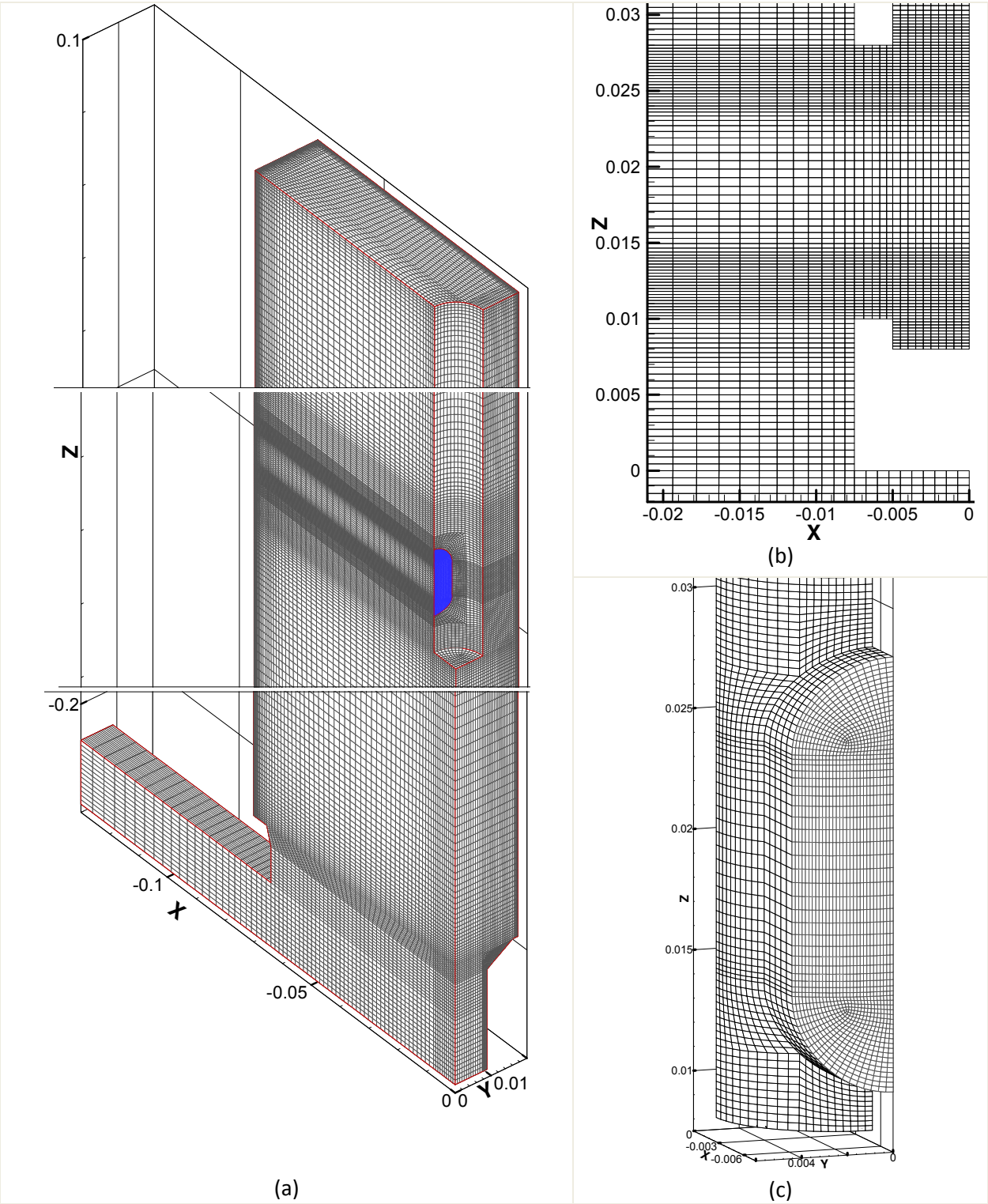

Fig-2 Typical nozzle and mold meshes used in RANS models (0.61 million cells in quarter domain) (a) mold mesh (b) close-up at the port in the mid-plane (c) mesh near nozzle port

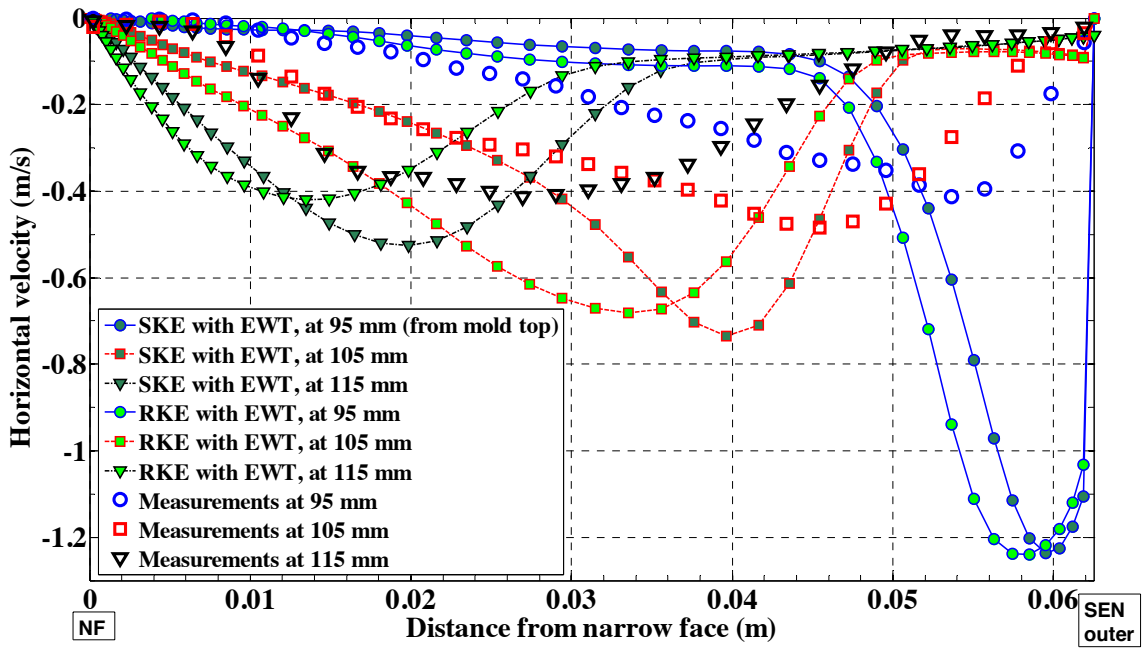

Fig-3 Comparison of average horizontal velocity predicted by RANS models (RKE and SKE) with the measurements

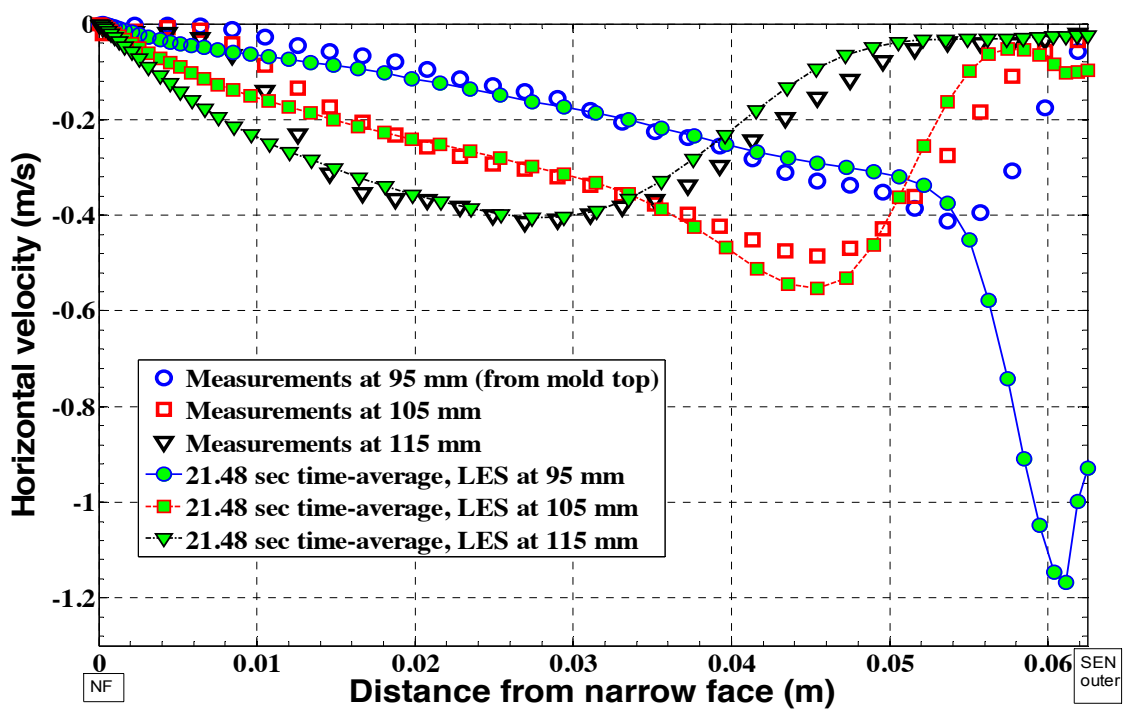

Fig-4 Comparison of average horizontal velocity predicted by LES with the measurements

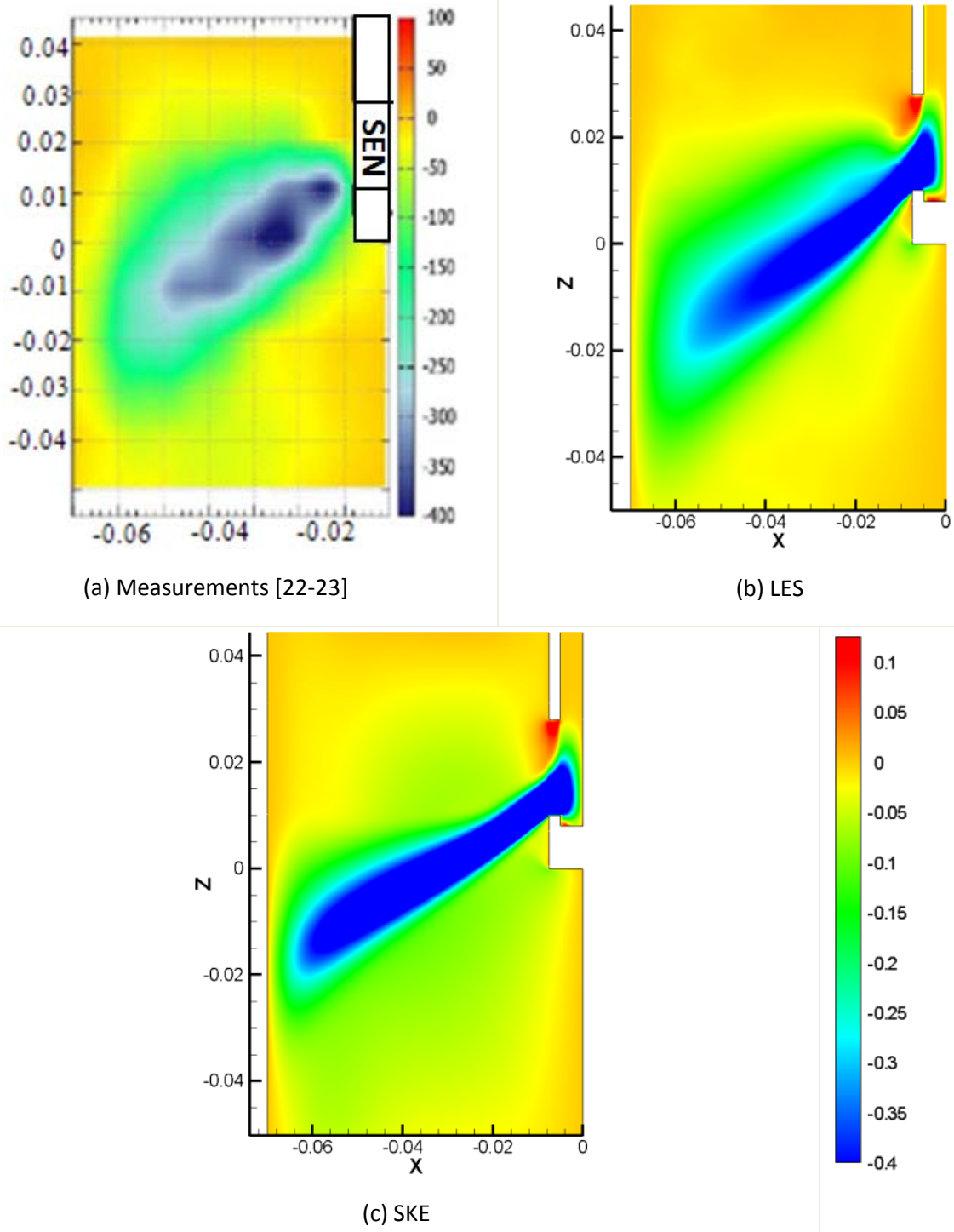

Fig-5 Average horizontal velocity contours in the mold mid-plane compared between (a) measurements (b) LES (21.48s time-average) and (c) SKE

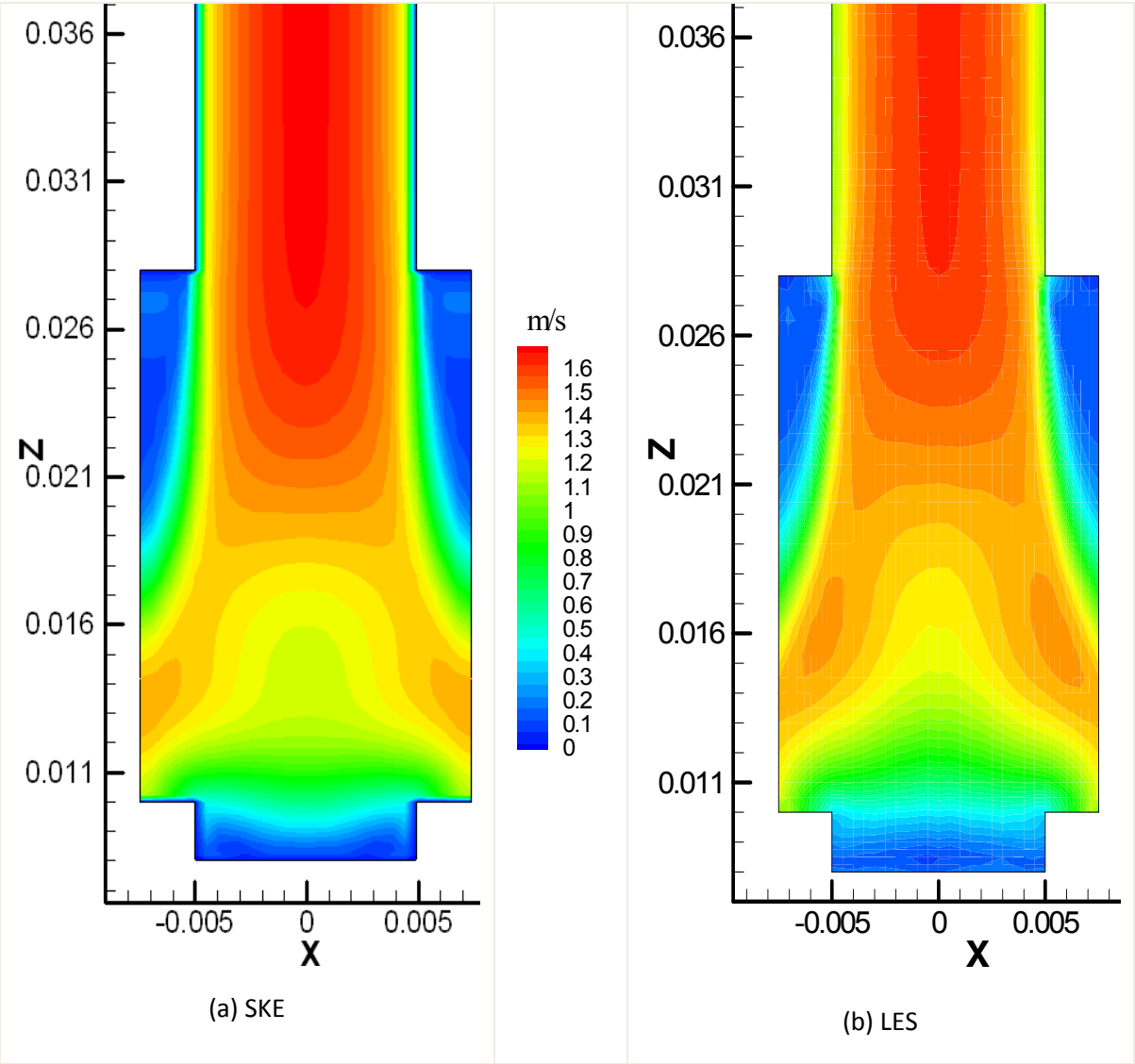

Fig-6 Average velocity magnitude contours in the nozzle mid-plane at the nozzle bottom compared in between (a) SKE and (b) LES

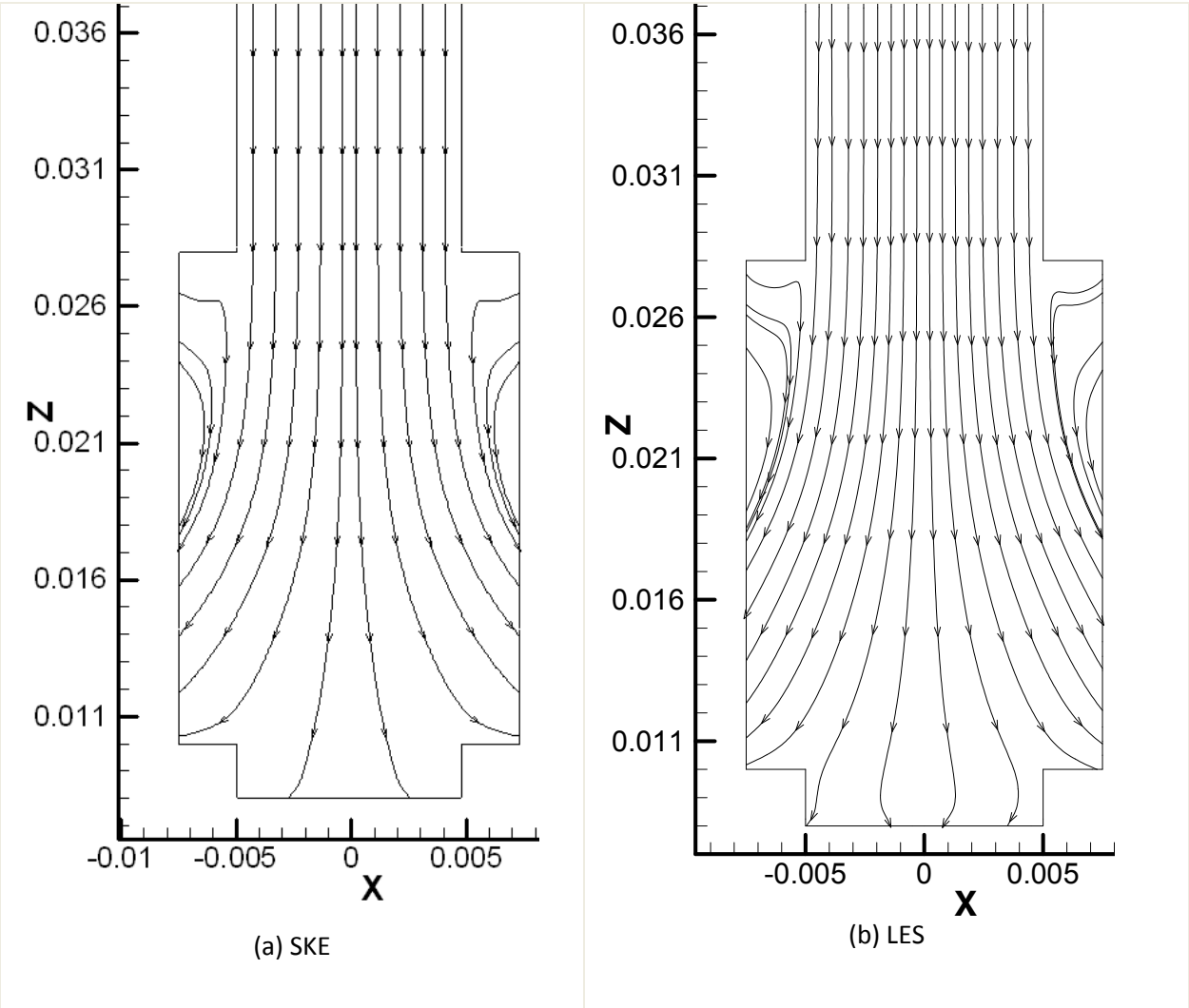

Fig-7 Streamlines in the nozzle mid-plane at the nozzle bottom compared in between (a) SKE and (b) LES

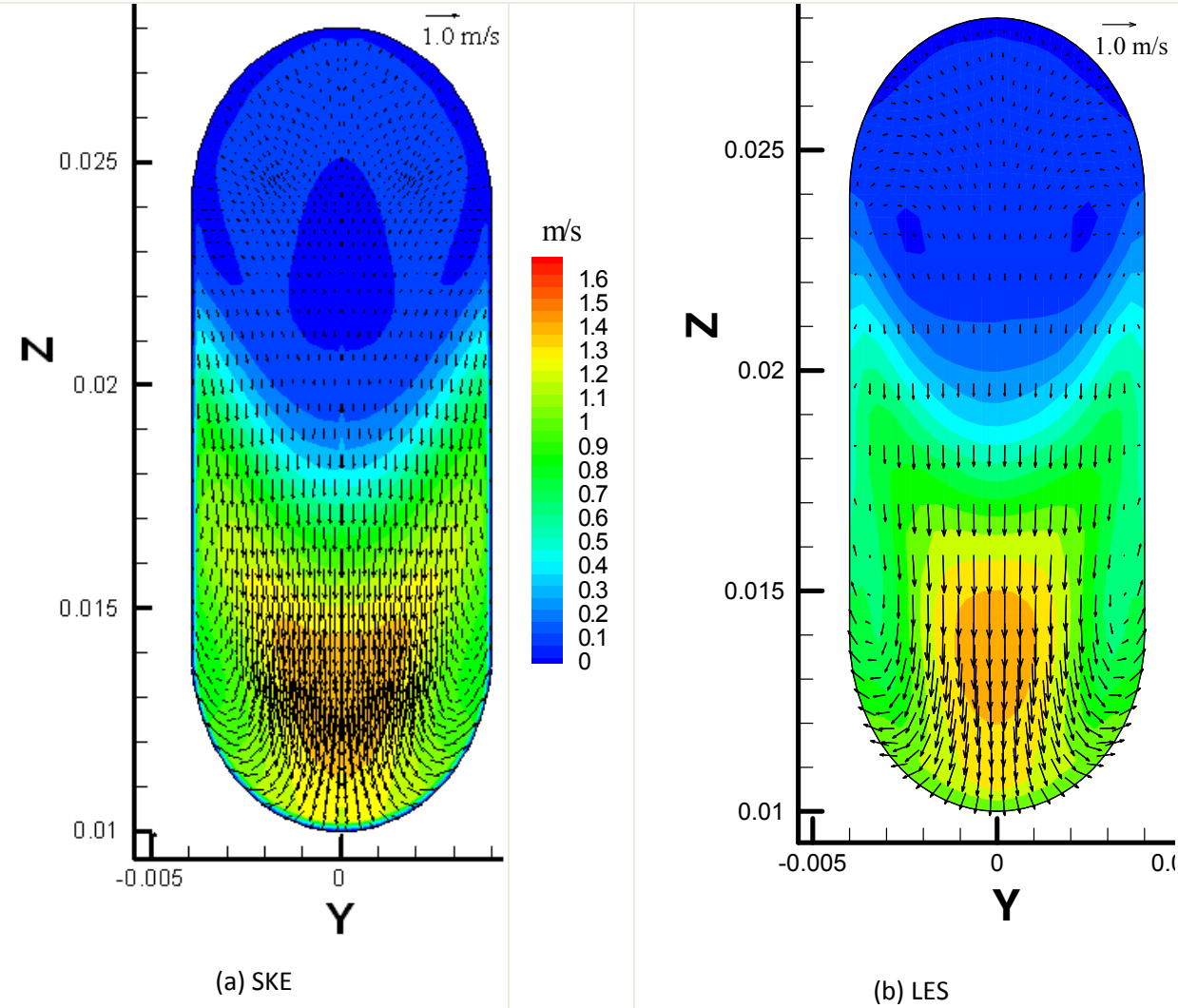

(a) SKE

(b) LES

Fig-8 Comparison of average port velocity magnitude and vectors (a) SKE and (b) LES (some of the vectors are skipped for better visualization)

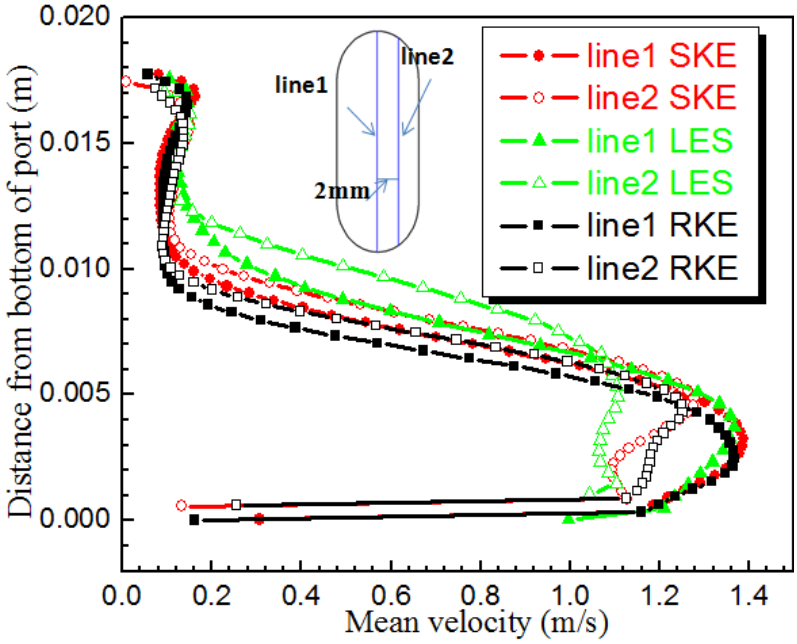

Fig.9 Comparison of port velocity magnitude predicted by RANS models (SKE and RKE) and LES

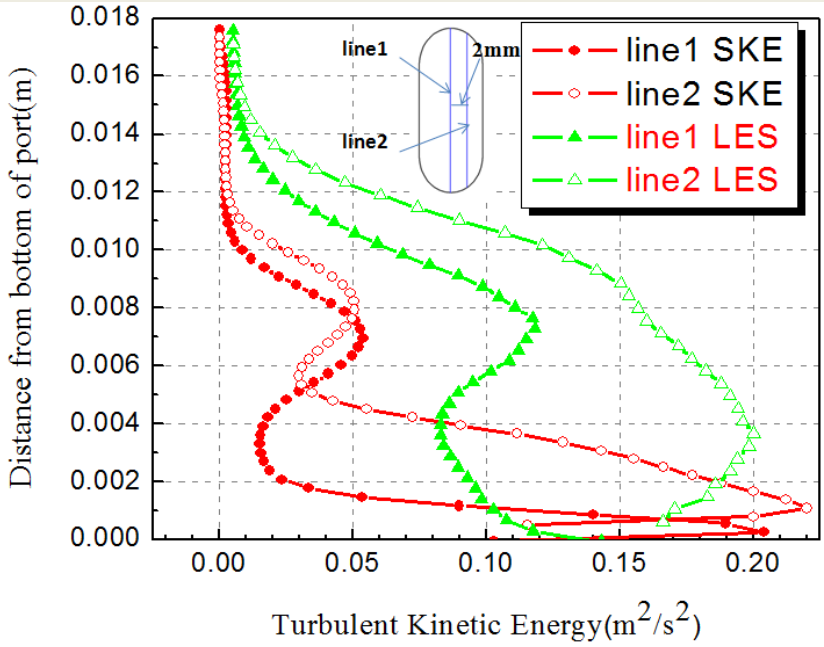

Fig10 Comparison of port turbulent kinetic energy in SKE and LES

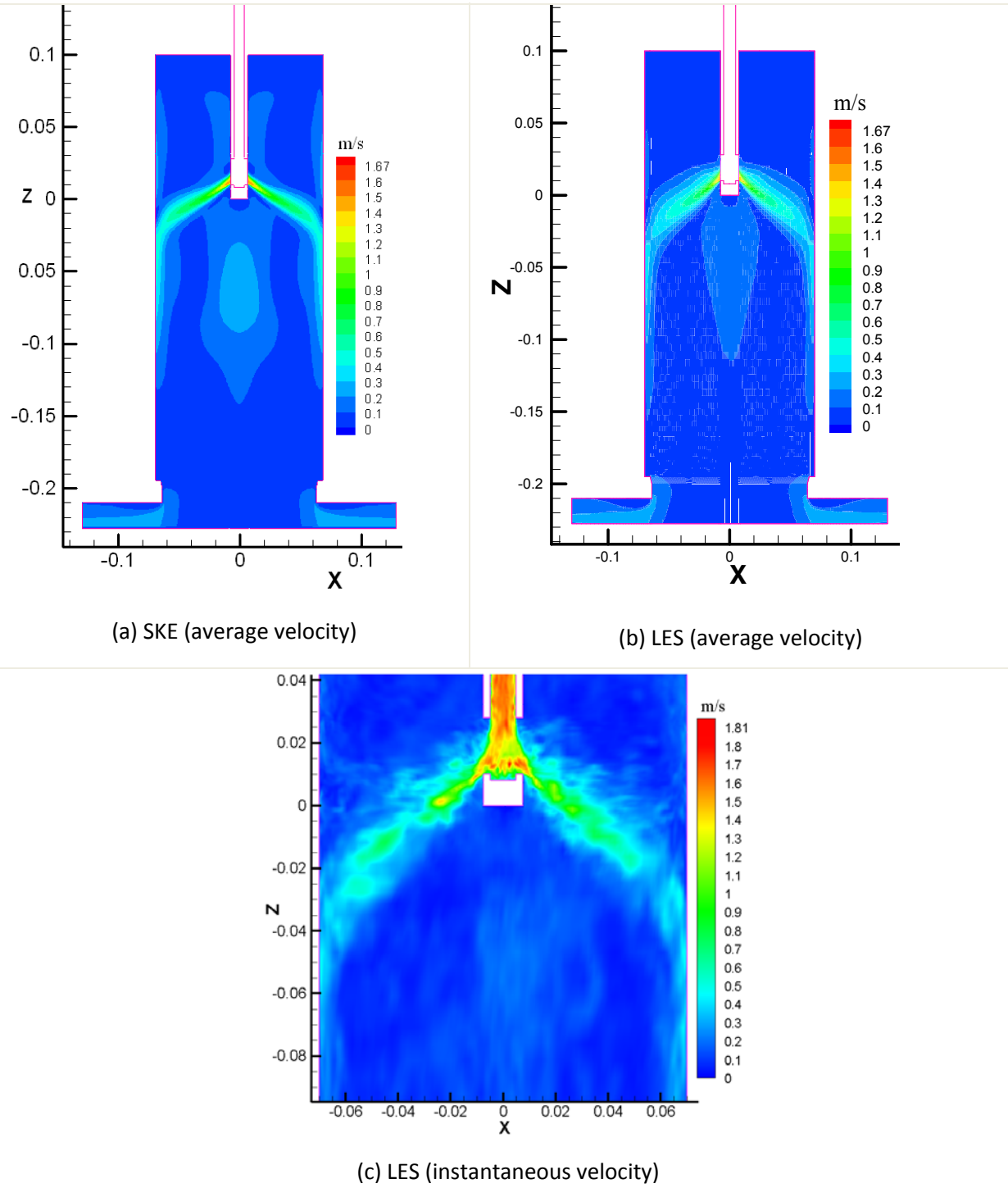

(a) SKE (average velocity)

(b) LES (average velocity)

(c) LES (instantaneous velocity)

Fig-11 Comparison of velocity magnitude at the mold mid-plane between wide faces (a) SKE (average velocity) and (b) LES (21.48 sec time average velocity) (c) Instantaneous velocity magnitude at 45.04 sec

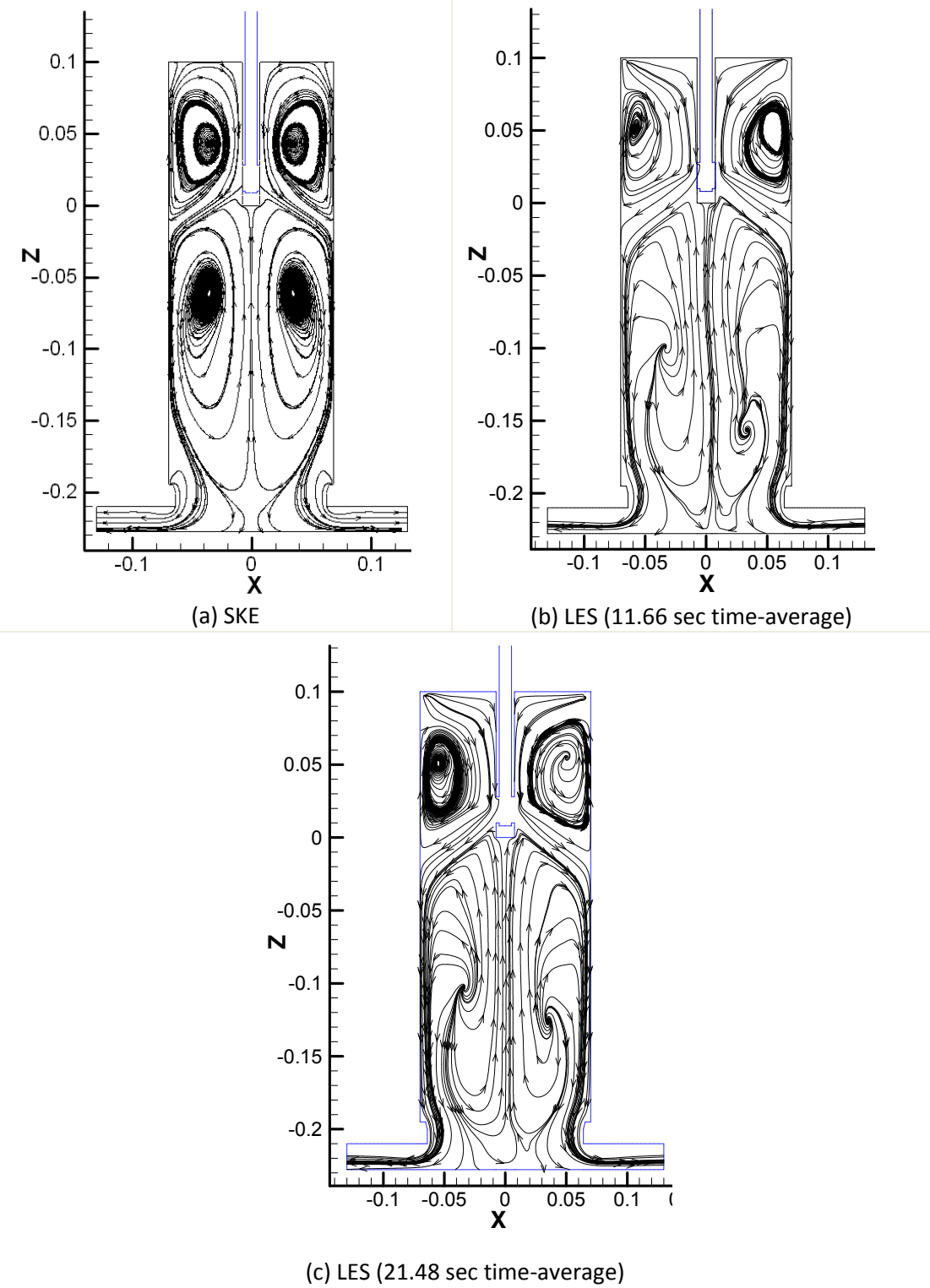

(a) SKE

(b) LES (11.66 sec time-average)

(c) LES (21.48 sec time-average)

Fig-12 streamlines at mold mid-plane in (a) SKE and (b) LES (11.66 sec time average) (c) LES (21.48 sec time average)

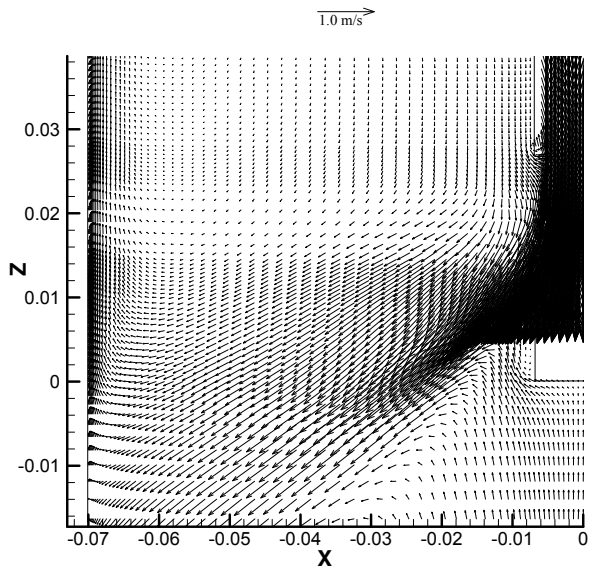

(LES, 21.48 sec time-average)

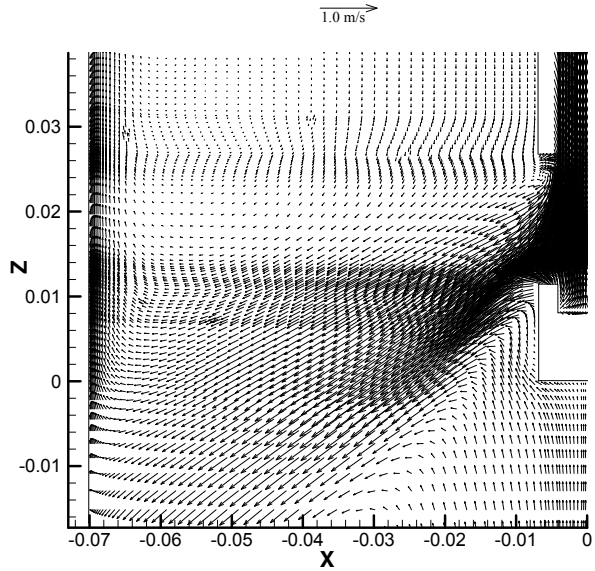

(LES, 21.48 sec time-average)

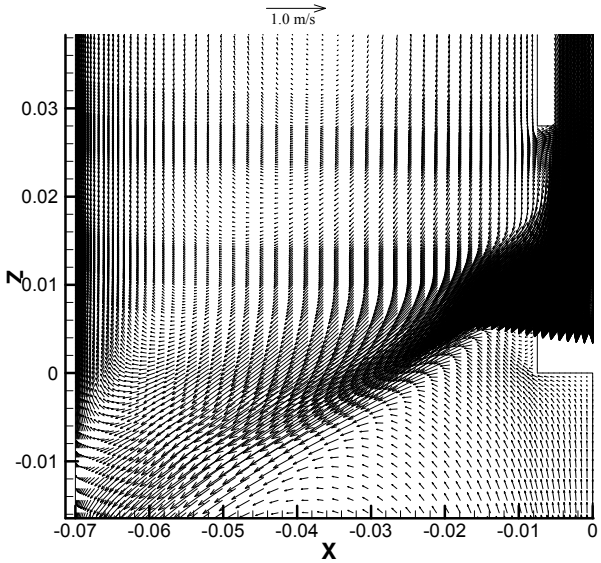

(SKE)

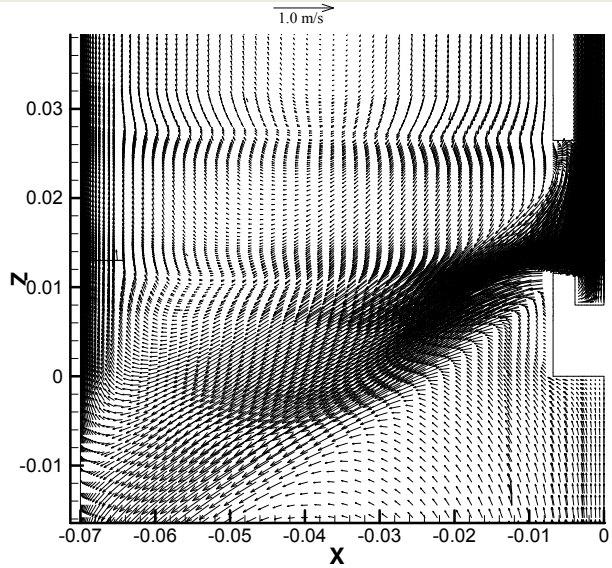

(SKE)

(a) mold-mid-plane between wide faces

(b) 3 mm towards wide face from mid-plane

Fig-13 Average velocity vectors at nozzle and mold (a) mid-plane (b) 3 mm towards wide face from mid-plane

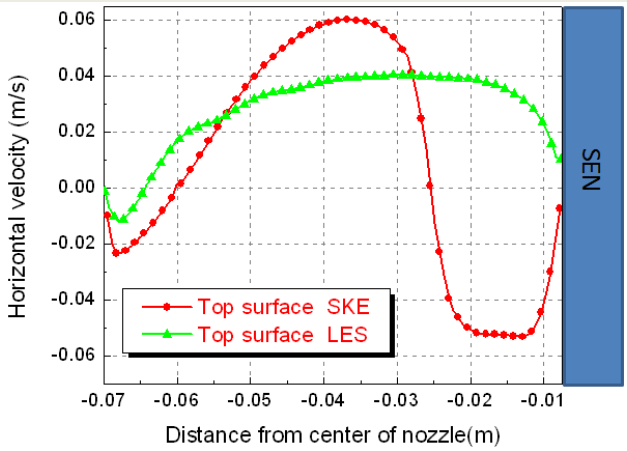

(a)

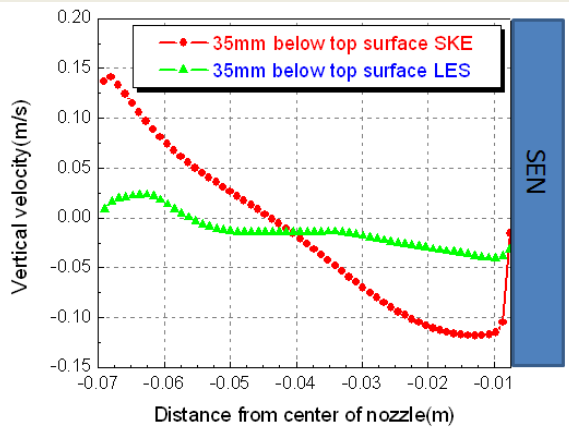

(b)

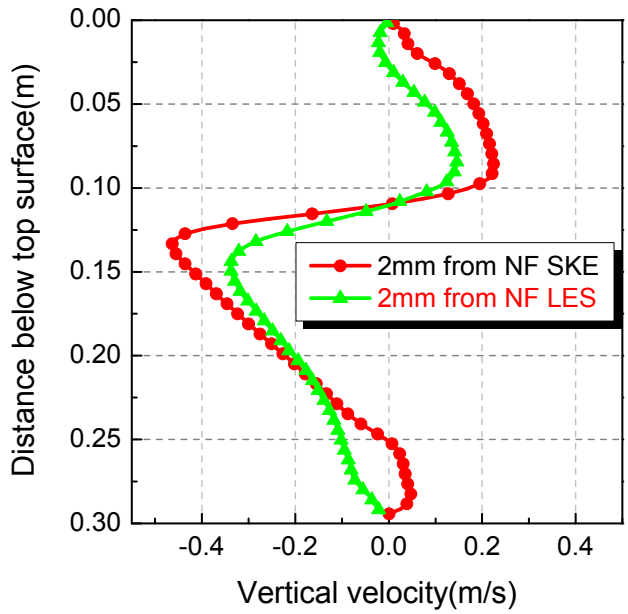

(c)

Fig-14 Comparison of velocity at mold mid-plane between LES and SKE (a)top surface horizontal velocity (b)35mm below top surface vertical velocity (c) vertical velocity at 2 mm from NF along mold length

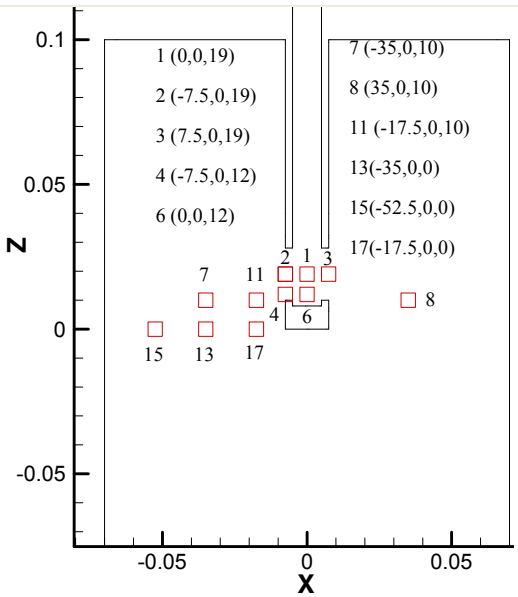
1 (0,0,19)
2 (-7.5,0,19)
3 (7.5,0,19)
4 (-7.5,0,12)
6 (0,0,12)
7 (-35,0,10)
8 (35,0,10)
11 (-17.5,0,10)
13(-35,0,0)
15(-52.5,0,0)
17(-17.5,0,0)
Z
X

(a)

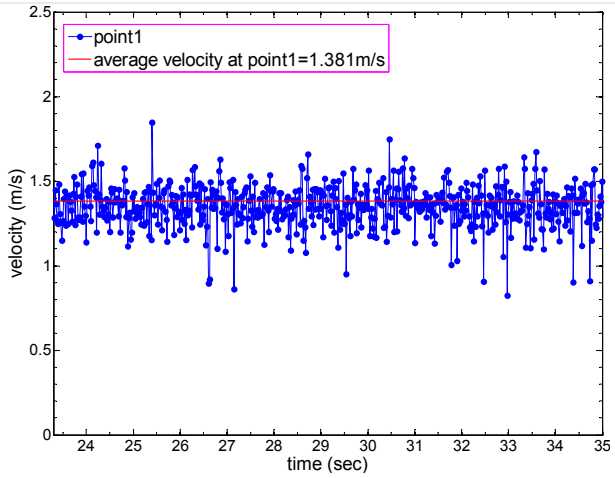
point1
average velocity at point1=1.381m/s
velocity (m/s)
time (sec)

(b)

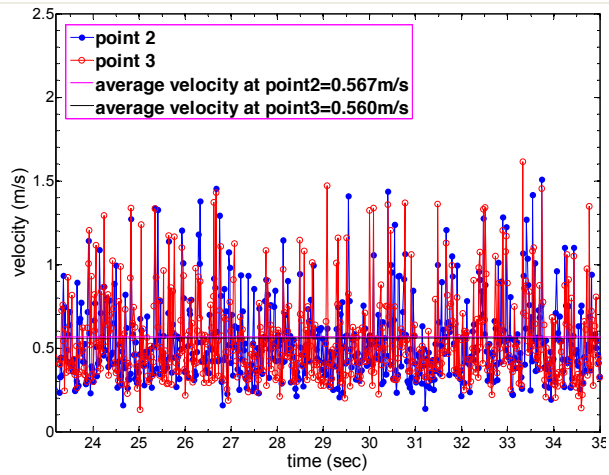
point 2
point 3
average velocity at point2=0.567m/s
average velocity at point3=0.560m/s
velocity (m/s)
time (sec)

(c)

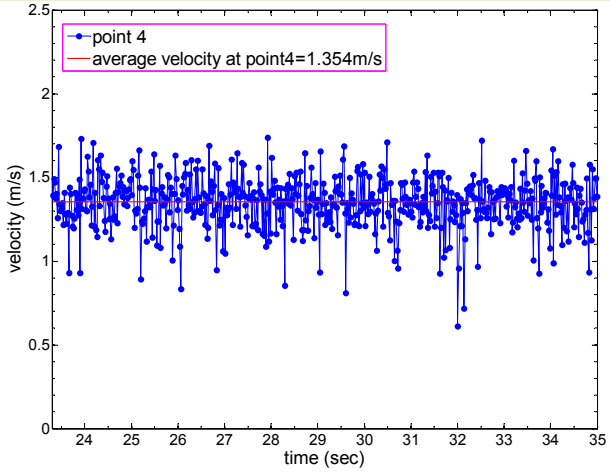
point 4
average velocity at point4=1.354m/s
velocity (m/s)
time (sec)

(d)

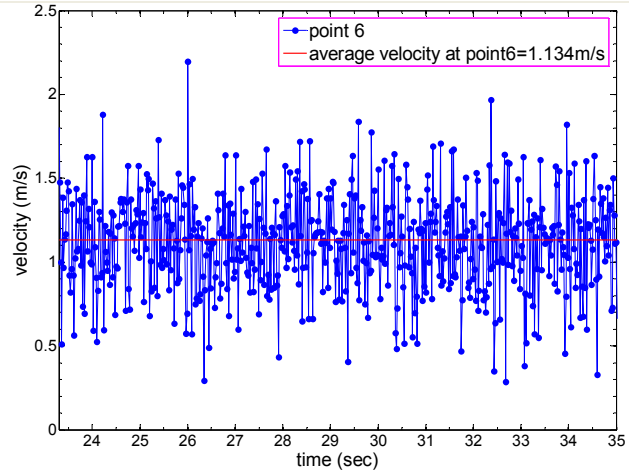
point 6
average velocity at point6=1.134m/s
velocity (m/s)
time (sec)

(e)

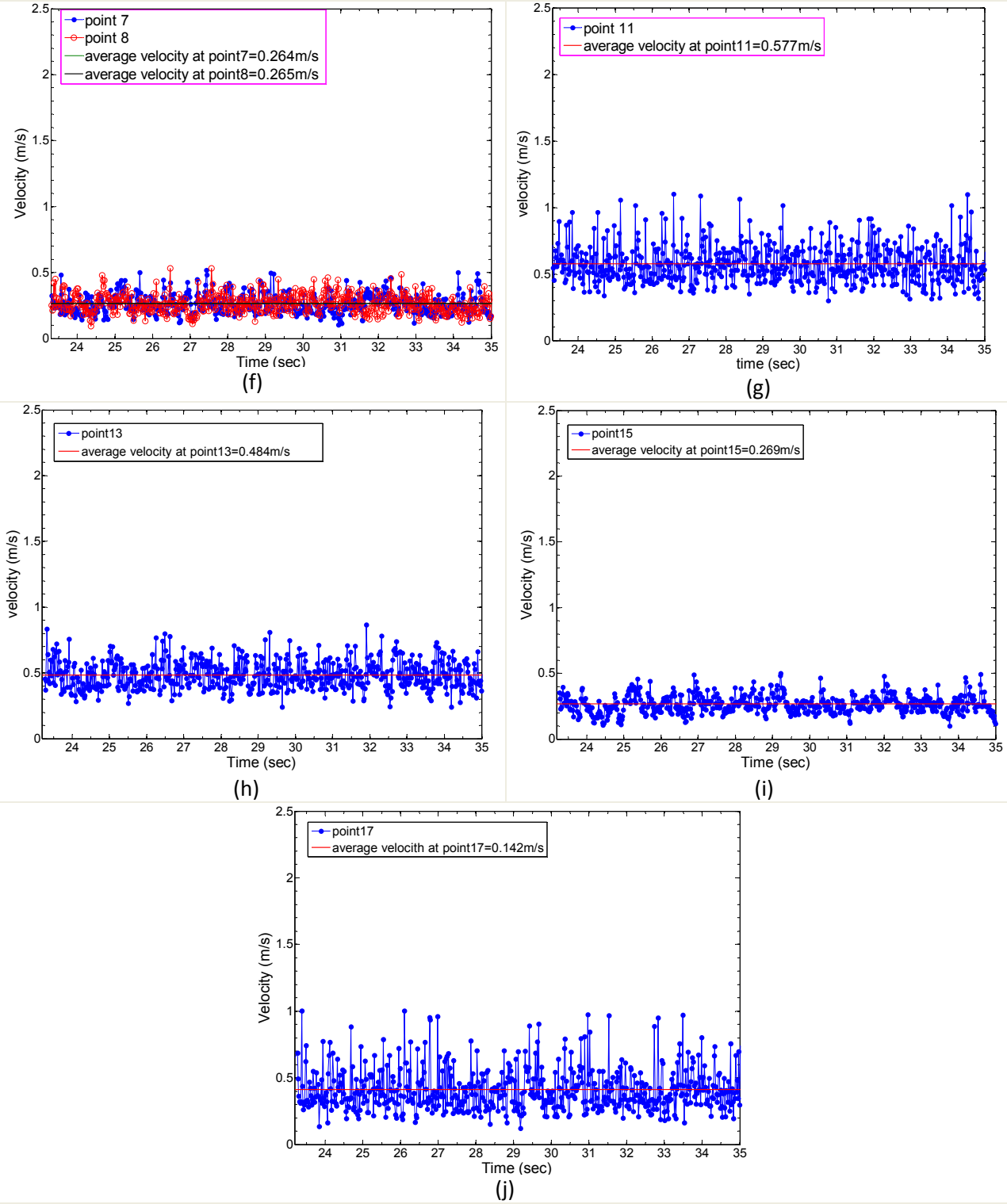

Fig-15 Velocity magnitude as a function of time at various points with point coordinates (given in mm) in the nozzle and mold mid-plane
(origin (0,0,0): is at nozzle bottom center mid-plane)

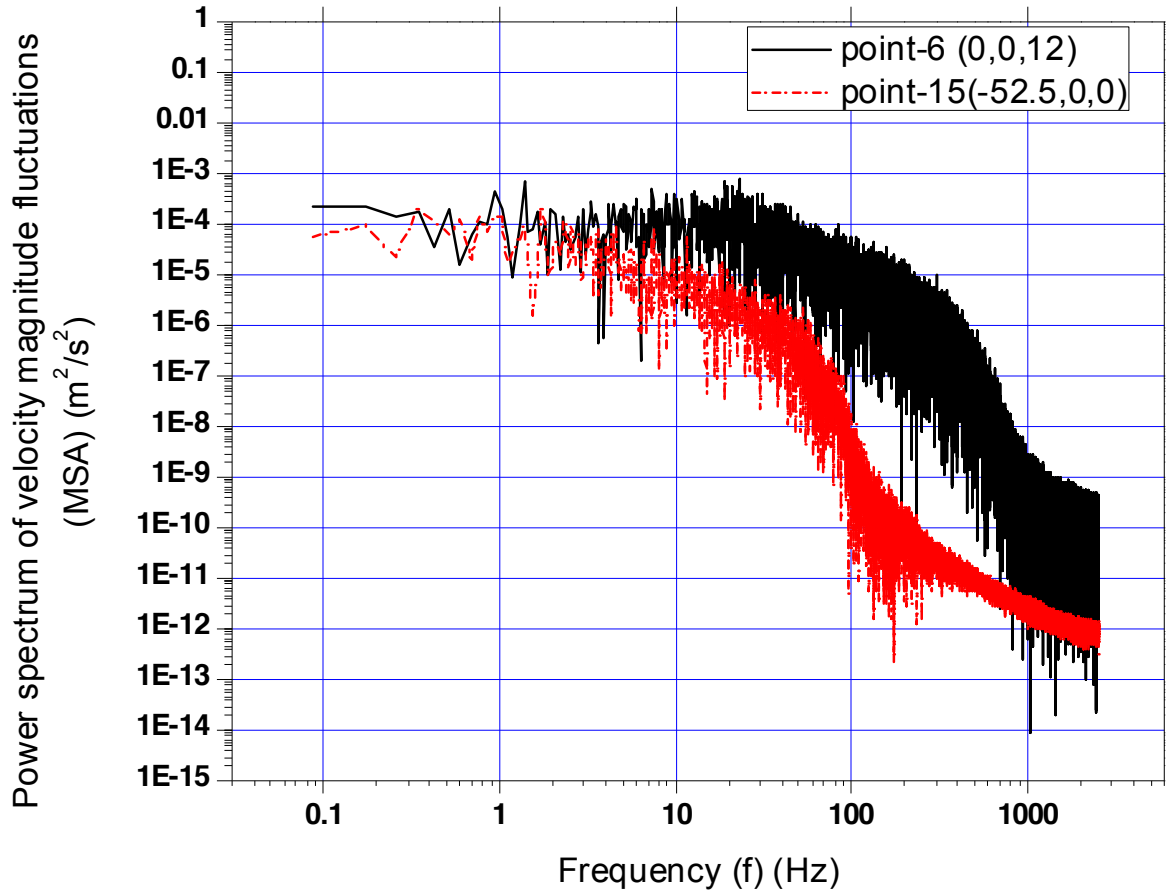

Fig-16 Power spectrum (Mean-Squared Amplitude(MSA)) of velocity magnitude fluctuations at two points (6 and 15) in the nozzle and mold at the mid-plane between wide faces

Table-1 Process parameters

Volume flow rate/ Nozzle inlet velocity	110 *ml/s* / 1.4 *m/s*
Casting speed	1.35 *m/min*
Mold width	140 *mm*
Mold thickness	35 *mm*
Mold length	330 *mm*
Nozzle diameter	10 *mm*
Total nozzle height	300 *mm*
Nozzle port dimension	8*mm*(width)×18*mm*(height) rectangular with top and bottom having 4 *mm* radius chamfered
Nozzle bore diameter(inner/outer)	10*mm*/15*mm*
SEN depth	72*mm*
Density(ρ)	6360 kg/m^3
Viscosity(μ)	0.001895 $kg/m\ s$
Nozzle port angle	0 degree
Shell	No
Gas injection	No

Table-2 Comparison of the jet characteristics in SKE and LES

Properties	SKE model	LES model
	Left port	Left port
Weighted average nozzle port velocity in x-direction(outward)(m/s)	0.816	0.71
Weighted average nozzle port velocity in y-direction(horizontal)(m/s)	0.073	0.108
Weighted average nozzle port velocity in z-direction(downward)(m/s)	0.52	0.565
Weighted average nozzle port turbulent kinetic energy (m^2/s^2)	0.084	0.142
Weighted average nozzle port turbulent kinetic energy dissipation rate (m^2/s^3)	15.5	---
Vertical jet angle (degree)	32.5	38.5
Horizontal jet angle (degree)	0	0
Horizontal spread (half) angle (degree)	5.1	8.6
Average jet speed (m/s)	0.97	0.91
Back-flow zone (%)	34.0	25.1